Desalination 617 (2026) 119425

Contents lists available at ScienceDirect

Desalination

journal homepage: www.elsevier.com/locate/desal

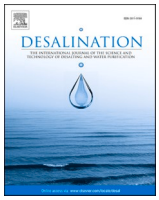

PFAS-contaminated groundwater treatment by forward osmosis using pressure-stimuli-responsive nanofiltration membrane: Effects of chain length and operating conditions

Yahia Aedan [a], Ali Altaee [a,*], Viktoria Mueller [b,c], Ho Kyong Shon [a], Lilyan Alsaka [a], Syed Javaid Zaidi [d]

[a] Centre for Green Technology, School of Civil and Environmental Engineering, the University of Technology Sydney, 15 Broadway, NSW, 2007, Australia
[b] The James Hutton Institute, Craigiebuckler, Aberdeen, AB15 8QH, United Kingdom
[c] Institute of Chemistry, University of Graz, Universitätsplatz 1, 8010, Graz, Austria
[d] Center of Advanced Materials, Qatar University, PO Box 2713, Doha, Qatar

HIGHLIGHTS

- Long, Short, & ultrashort-chain PFAS removal increased at alkaline feed pH.
- PFAS rejection was in the following order: ultrashort<short<long-chain.
- The highest PFAS rejection was achieved at pH 9 & 4 bar feed pressure.
- Maximum removal of long, short, & ultrashort-chain was 99–100 %, 97–98 %, & 91.4 %.

ARTICLE INFO

Keywords:
PFAS
Membrane
Pressure stimuli-responsive membrane
Groundwater
Ultra-short-chain PFAS
Heavy metals

ABSTRACT

Significant health concerns have been raised resulting from the increasing detection of *per*- and polyfluoroalkyl substances (PFAS) in various water bodies. Attention has shifted beyond long-chain compounds, carbon-chain length ≥ C7, to include the more mobile and persistent short, carbon-chain length C4-C6, and ultra-short-chain PFAS, carbon-chain length C1-C3. This study systematically investigated the rejection of PFAS-contaminated groundwater using a pressure-stimuli-responsive nanofiltration (PSRNF) membrane with varying pressures and pH of the feed solution. The rejection efficiency of long- and short-chain PFAS by the PSRNF membrane increased with both increasing pressure and pH, achieving 99.1 % to 100 % for long chains and 96.9 % to 98 % for short chains. In contrast, the ultra-short-chain PFAS rejection efficiency by the PSRNF membrane decreased at acidic pH with increasing pressure, but increased at alkaline pH, achieving up to 91.4 %. There was a higher tendency for membrane adsorption of long-chain PFAS due to strong hydrophobic interactions at low pressure, resulting from a longer contact time with the membrane. Ultra-short-chain PFAS exhibited no adsorption across all conditions due to their low hydrophobicity and minimal affinity for the membrane surface. This performance was closely linked to both the physicochemical properties of the PFAS species and the operational environment, such as pH and applied pressure. These findings highlight both the practical benefits of the PSRNF membrane and the importance of optimising operating conditions for effective removal of PFAS and heavy metals from contaminated water.

1. Introduction

Per- and polyfluoroalkyl substances (PFAS) are synthetic, highly fluorinated chemicals that have been employed for over seventy years throughout many products and industrial processes, including fire-fighting foams, semiconductors, textiles, packaging, and other applications [1,2]. Over the past decade, due to their proven bioaccumulative nature with consequent harmful effects on living organisms [3],

* Corresponding author.
E-mail address: ali.altaee@uts.edu.au (A. Altaee).

https://doi.org/10.1016/j.desal.2025.119425
Received 7 August 2025; Received in revised form 3 September 2025; Accepted 17 September 2025
Available online 18 September 2025

regulatory frameworks surrounding the most prevalent long-chain PFAS, such as perfluorooctanoate (PFNA) and Perfluorooctanoic acid (PFOA), have become progressively more stringent worldwide. These substances are now classified as high-concern chemicals, resulting in their restrictions. The phase out of some legacy PFAS, such as Perfluorooctanoic acid (PFOA) and Perfluorooctane sulfonic acid (PFOS), with a C8 carbon chain, has resulted in a shift toward short-chain PFAS, typically characterised by carbon chain lengths of C6 or fewer for carboxylic acids, such as Perfluorohexanoic acid (PFHxA) and C5 or fewer for sulfonic acids, such as perfluorobutanesulfonate (PFBS) and Perfluorobutanoic acid (PFBA) with a C4 carbon chain [4,5]. Ultrashort-chain perfluoroalkyl acids contain three or fewer carbon atoms ($\leq$ C3), e.g., trifluoroacetic acid (TFA) with C2 and perfluoropropanoic acid (PFPrA) with C3, are perfluoroalkyl acids and have received considerably less attention from researchers than short-chain PFAS. The prevalence of short-chain PFAS in the environment is primarily associated with the substitution of legacy C8 compounds by C6–C4 alternatives, such as PFBS and PFBA, which are directly implemented in numerous commercial applications, including ski waxes, leather treatments, and aqueous film-forming foams (AFFFs) [6].

Addressing complex scenarios of pollution, including the coexistence of long, short and ultrashort chain PFAS, each with a unique structure, hydrophobicity, and electrostatic charges, poses further challenges for treating contaminated water. This study is focused on the treatment of PFAS-contaminated groundwaters that are contaminated with ultrashort-, short-, and long-chain PFAS that reach groundwaters near industrial facilities and firefighting training sites as a result of widespread use and leaching, landfills, and the degradation of precursor chemicals used in products. These sources introduce different chains of PFAS that would migrate and persist in groundwater in complex mixtures that are challenging to treat. Compared to traditional techniques, high-pressure driven membrane filtration technologies are an effective approach for addressing water sources contaminated with PFAS, where the small pore size of reverse osmosis (RO) and nanofiltration (NF) membranes promotes their molecular cut-offs (MWCO) to be sufficient to reject most PFAS of interest [7]. The major mechanisms for PFAS rejection by the NF and RO membranes are size exclusion and electrostatic repulsion, while mechanisms such as hydrophobic interaction, adsorption on the membrane, and Donnan exclusion also contribute to PFAS rejection [8]. Liu et al. indicated that the removal efficiency of Perfluoropropane sulfonic acid (PFPrS) (ultrashort-chain) reached 90–93 % by the NF membrane (subject to water flux), whereas the Filmtec NF270 membrane maintains more than 97 % removal efficiency for long-chain Perfluorooctanoic Acid (PFOA) and Perfluorooctane Sulfonic Acid (PFOS) from contaminated groundwater [9]. Another study reported that the removal efficiencies for ultrashort-chain PFAS (PFBA) and short-chain PFAS (PFHpA) were 86.1–98.1 % and for long-chain (PFOS) was 99 % using a layer-by-layer laboratory-assembled NF membrane [10]. Although the RO and NF membranes demonstrate high rejection efficiency for PFAS-contaminated water, they still require high energy for operation, which escalates the treatment cost and leads to higher greenhouse gas emissions. Furthermore, membrane fouling remains a critical challenge in filtration processes, as it compromises membrane durability and contributes to elevated operational expenses.

To address these limitations, a pressure stimulus-responsive NF (PSRNF) membrane is a novel technology that aims to enhance separation efficiency while overcoming critical operational issues, such as energy consumption and fouling [11]. The membrane operates on the principles of forward osmosis (FO), where water movement is osmotically induced by the draw solution and enhanced by the application of low hydraulic pressure on the feed side, subsequently enhancing water flux. A recent study has shown the significant efficacy of PSR membranes in removing PFOA from contaminated wastewater [12]. The PSRNF membrane demonstrated a PFOA rejection efficacy of 99.1 %, along with superior water permeability, fouling resistance, minimal energy consumption, and cost-effectiveness relative to the other FO membranes [12].

Considering the recent findings that demonstrate a high PFOA rejection rate and the resilience of the PSRNF membrane. This study systematically evaluated the PSRNF membrane for treating PFAS-contaminated groundwater. The investigation includes a variety of PFAS compounds (long, short, and ultrashort chains) that exist in the polluted groundwater. In order to investigate the influence of operational conditions on PSR membrane performance, the study examined i) the effects of applied hydraulic pressure and feed solution pH on a variety of PFAS species rejection, ii) the adsorption behaviour of PFAS onto the membrane surface under varying operational conditions, iii) the preferential PSRNF membrane rejection of long, short, and ultra short PFAS compounds in groundwater, and iv) the membrane performance on multiple filtration cycles, addressing fouling propensity and mitigation methods. By integrating PFAS rejection, adsorption behaviour, and heavy metal filtration, this study provides a holistic evaluation of the PSR membrane's capabilities for addressing complex and heterogeneous water pollution scenarios.

2. Materials and methods

2.1. Chemicals and materials

All chemical reagents employed for this study were of analytical grade. Sodium chloride (NaCl, 99 % purity), sodium hydroxide (NaOH, 99 % purity), and hydrochloric acid (HCl, 37 % purity) from Sigma-Aldrich (Australia). Analytical-grade standards used for PFAS quantification included PFAC30PAR reference standard solution, containing 30 PFAS substances, for calibrating HLPC and LC instruments, and an isotopically labelled internal standard MPFAC-HIF-ES for improving the accuracy and reliability of PFAS analysis (Wellington Laboratories, Canada). Ultrapure water with a resistivity of 18 MΩ·cm was produced using a Millipore purification system (Merck). LC/MS-grade ammonium acetate (CH_3COONH_4) was sourced from Fischer Chemicals, Austria, while methanol and acetonitrile of LC/MS grade were procured from Bartelt, Austria. A commercially available thin film flat sheet polyamide TS80 NF membrane from TRISEP® was incorporated for the filtration experiments. PFAS-contaminated groundwater sourced from a heavily contaminated site in NSW, Australia, was the feed solution in the FO process using a PSRNF membrane. The draw solutions used included a 0.6 M sodium chloride (NaCl) solution (prepared by dissolving 35.06 g of NaCl in one litre of DI water) and natural seawater collected from Sydney, Australia.

2.2. Targeted analysis with LC-ESI-MS/MS

For PFAS with chain length C4 and above, a Shimadzu high-performance liquid chromatography (HPLC, Shimadzu, Japan) system equipped with a Kinetex EVO C18 column (5 μm, 2.1 × 100 mm; Phenomenex) was used for analyte separation. For PFAS with chain length C4 and above, a Shimadzu high-performance liquid chromatography (HPLC, Shimadzu, Japan) combined with a Kinetex EVO C18 column (5 μm, 2.1 × 100 mm; Phenomenex) was used for the separation of the analytes by LC. A gradient elution method was applied for the separation of target PFAS, employing 5 mmol L^{-1} CH3COONH4 in ultrapure water and 100 % LC-MS grade methanol (MeOH) as mobile phases A and B. For the analysis of ultrashort-chain PFAS (C $\leq$ 3), the same HPLC was combined with a Raptor Polar X (2.7 μm, 2.1 × 50 mm, Restek, Germany) with a gradient elution, consisting of the same mobile phases. The LC system in both cases was coupled to a Shimadzu tandem mass spectrometer (MS/MS) (Shimadzu, Japan). Mass spectrometric analysis was conducted in negative electrospray ionization mode using multiple reaction monitoring (MRM). For most target analytes, two transitions were tracked, one serving as the quantifier ion and the other as the qualifier. To accommodate the extensive number of MRM transitions, data acquisition was restricted to time segments corresponding to each

compound's retention window. Each sample was spiked with 50 μL of 1000 pg g^{-1} isotopically labelled internal standard. A ten-point calibration curve, covering concentrations from 100 to 2000 pg g^{-1} in methanol, was prepared and analysed during the run. The lowest calibration points with a signal-to-noise ratio greater than 3 were set as the instrumental limit of detection (LOD), and the lowest calibration points with signal to noise ratio greater than 10 were set as the limit of quantification (LOQ). Concentrations were calculated based on the ratio between the analyte and the isotopically labelled internal standard.

2.3. Sample preparation for PFAS detections

2.3.1. Water samples

100 μL of the water sample (draw and feed solutions) was diluted with 400 μL of a 50:50 *v*/v methanol solution, then 100 μL of a 1000 pg g^{-1} isotopically labelled internal standard was added. The solution was shaken vigorously and then transferred into a clean LC vial for analysis. Three method blanks were included in the analysis, and in cases where PFAS signals were detected in the method blanks, the mean peak area from the blanks was subtracted from the corresponding sample measurements to correct for background contamination.

2.3.2. Membranes

After each experiment, the membrane was replaced and prepared for PFAS analysis. One membrane from each run was cut in half, then one of the halves was placed into a 15 mL centrifuge tube and spiked with 200 μL of a 1000 pg g^{-1} isotopically labelled internal standard solution and 20 μL of a 50,000 pg g^{-1} isotopically labelled trifluoroacetic acid (TFA) solution. The membrane samples were then extracted using 15 mL of 0.1 % *v*/v ammonium hydroxide (NH_4OH) in methanol using a shaker at 320 rpm (rpm) for 1 h. Following extraction, the tubes were then centrifuged, and an aliquot was transferred into LC vials for instrumental analysis. To ensure accuracy, three method blanks (unused membranes of the same type) were included in the analysis. If PFAS compounds were detected in the blanks, the average blank signal area was subtracted from the corresponding sample results to correct for background contamination.

2.4. Membrane, groundwater and seawater characterisations

The PSRNF TS80 membrane is a commercially available flat sheet membrane with a thin film polyamide that is commonly used as a softening membrane in various water treatment applications. The membrane was selected in the FO process due to its high tolerance to a wide range of pH (2−12) and its low structural parameter (130–177 μm) (Table S1), which reduces internal concentration polarisation. It also has an excellent water permeability coefficient (Aw) of 13.1 L/m^2h.bar, salt permeability coefficient (B) of (2.38 L/m^2h for NaCl, and 0.69 L/m^2h for $MgSO_4$) (Supplementary S1), and hydrophilic surface characteristics [12]. Field Emission Scanning Electron Microscopy (FE-SEM) was conducted employing a Zeiss EVO LS15 SEM system (Zeiss, Australia) to examine the surface characteristics of the membrane samples. Prior to SEM analysis, all membrane samples were coated with a thin layer of chromium (~5 nm) using a sputtering system (Leica EM ACE600) operated at a current of 30 mA, in order to mitigate charging effects associated with the non-conductive membrane surfaces. Elemental composition was further characterised through Energy Dispersive X-ray (EDX) spectroscopy, conducted using a Bruker SDD XFlash 5030 detector integrated with the Zeiss EVO LS15 SEM system (Zeiss, Australia). Membrane surface characterisation was conducted through Fourier Transform Infrared (FT-IR) spectroscopy to identify surface functional groups before and after the experimental procedures. A Thermo Scientific Nicolet 6700 FT-IR spectrometer was employed for this analysis. Prior to measurement, membrane samples were thoroughly dried, and spectra were collected at a minimum of three different points on each sample to ensure repeatability and representativeness of the results. Groundwater and seawater samples were analysed using the Agilent 8900 Triple Quadrupole Inductively Coupled Plasma Mass Spectrometer (ICP-QQQ), a high-precision instrument designed for trace elemental analysis. The results of this analysis of the groundwater and seawater are presented in Table 1. The groundwater feed solution contained 11 detectable PFAS species, including long, short, and ultra-short-chain species, with their concentrations prior to the filtration treatment shown in Table 2.

2.5. Experiment setup

A laboratory-scale filtration system was employed to assess the operational efficiency of the PSRNF TS80 membrane in the purification of contaminated groundwater under various operational situations (Fig. 1). The system configuration comprised a transparent acrylic filtration cell (model CF042A-FO, Sterlitech) with a membrane filtration area of 42 cm^2, each side of the membrane possessing an internal volume of 17 mL. Two gear pumps (Cole-Parmer) were used, one pump on the feed side and the other on the draw, operating at a constant flow rate of 2 L/min to maintain constant crossflow conditions throughout the experiment. A pressure gauge (USG, USA) was attached to the feed line to control and observe the applied hydraulic pressure manually. Flow rates on both sides were monitored using F-550 series flow meters manufactured by Blue-White Industries. To quantify water transport across the membrane, the feed solution beaker was positioned on a high-precision digital balance (A&D EK-15KL), connected to a computer system that continuously recorded the reduction in mass on the feed beaker, indicative of the volume of water permeating through the membrane into the draw solution. Conductivity and total dissolved solids (TDS) were quantified in both the feed and draw solutions before, during, and after each run using a portable metre (HQ14d, HACH, Australia). Samples from the feed and draw solution compartments were collected at the commencement and conclusion of each experiment and stored at 3 °C for further analysis. All experiments were conducted at room temperature (about 23 °C).

Table 1
Seawater and groundwater characteristics.

Parameter	Measurement instrument	Seawater	Groundwater
Conductivity	LAQUA meter (Horiba, Japan)	50.2 ± 1 ms/cm	0.704 ± 3 ms/cm
Total Organic Carbon	TOC Analyser (Shimatzu, Japan)	2.4 ± 0.5 mg/L	11.7 ± 0.5 mg/L
Total dissolved Solids	LAQUA meter (Horiba, Japan)	29,500 ± 100 mg/L	340.2 ± 0.5 mg/L
pH	LAQUA-pH meter (Horiba, Japan)	7.1	4
Mn	ICP-MS (Agilent, United States)	85 ± 0.5 mg/L	9.7 ± 0.1 mg/L
Si	ICP-MS (Agilent, United States)	0.151 mg/L	10 ± 0.5 mg/L
K	ICP-MS (Agilent, United States)	338 ± 1 mg/L	14.9 ± 0.1 mg/L
Mg	ICP-MS (Agilent, United States)	1151.5 ± 4 mg/L	7.9 ± 0.3 mg/L
Cl	ICP-MS (Agilent, United States)	1858.5 ± 3 mg/L	33.5 ± 2 mg/L
Ca	ICP-MS (Agilent, United States)	320 ± 5 mg/L	6.8 ± 0.1 mg/L
Na	ICP-MS (Agilent, United States)	10,850 ± 3 mg/L	45 ± 2 mg/L
Al	ICP-MS (Agilent, United States)	5.2 ± 0.2 μg/L	12.8 ± 0.1 mg/L
Fe	ICP-MS (Agilent, United States)	2.9 ± 0.3 μg/L	11.5 ± 0.2 mg/L
Cu	ICP-MS (Agilent, United States)	3.4 ± 0.3 μg/L	1.71 ± 0.02 mg/L
Zn	ICP-MS (Agilent, United States)	1.3 ± 0.2 μg/L	1.97 ± 0.1 mg/L

Table 2
PFAS species and concentrations detected in the groundwater. Segregation of PFAS compounds according to their molecular weight (MW): long-chain >364 MW, short-chain >214–364, and ultrashort-chain ~114–250 MW.

Compound Name	Acronym	Molecular Weight g/mol	Groundwater Concentration ng/L	pKa	Structure
Trifluoroacetic acid	TFA	114	910 ± 15	0.23[13]	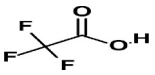
Trifluoromethanesulfonic acid	TFMS	150	1775 ± 20	- 14[14]	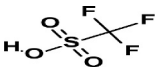
Perfluoropropanoic acid	PFPrA	164	2320 ± 22	0.38[15]	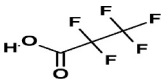
Perfluoropropanesulfonic acid	PFPrS	250	546 ± 12	−3.63[15]	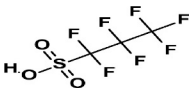
Perfluorohexanoic acid	PFHxA	314	2830 ± 25	- 0.16[16]	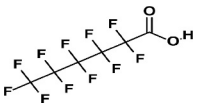
Perfluoroheptanoic acid	PFHpA	364	1220 ± 20	0.47[11]	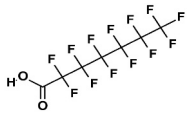
Perfluorohexanesulfonic acid	PFHxS	400	3587 ± 15	–	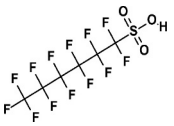
Perfluorooctanoic acid	PFOA	431	1741 ± 11	3.8[17]	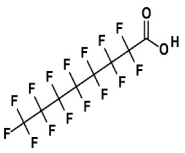
Perfluorononanoic acid	PFNA	464	1434 ± 15	0.5[13]	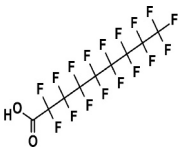
Perfluorooctanesulfonic acid	PFOS	500	1109 ± 8	−3.3[18]	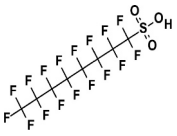
Perfluorodecanoic acid	PFDA	514	894 ± 9	0.52[13]	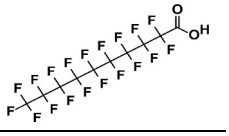

2.6. Water permeation flux and rejection analysis

The permeation flux, representing the rate at which water traverses the membrane from the feed to the draw solution, was determined by measuring the change in the feed solution's weight over time using the following equation:

$$F_w = \frac{\Delta W}{A^* \Delta t} \quad (1)$$

Fw represents the permeation flux of the membrane (L/m^{2}h), ΔW corresponds to the change in feed solution mass in kg, A is the effective membrane area in m^2, and Δt is the duration of the filtration process measured in hours (h). The rejection efficiency (R_E) of the membrane, presented as a percentage, was evaluated using the equation provided below:

$$R_E = \left(1 - \frac{C_d}{C_f}\right) \times 100 \quad (2)$$

Where C_d and C_f represent the solute concentration of the draw solution

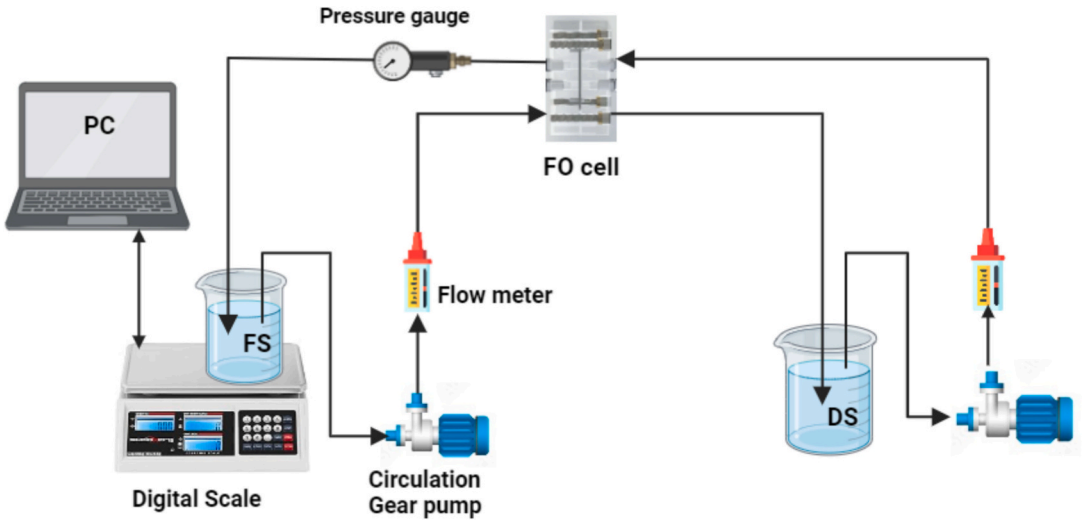

Fig. 1. Laboratory-scale forward osmosis filtration system.

and feed solution of contaminants in (ng/L), respectively.

2.7. Membrane cleaning studies

Membrane cleaning was conducted by circulating 40 °C DI water at a flow rate of 3 LPM on both sides of the membrane for 30 min. The groundwater filtration cycle involved one litre of contaminated groundwater at 4 bar applied pressure and pH 7 as the feed solution, while the seawater was the draw solution. Filtration experiments are set to stop when a 90 % recovery rate is reached. To evaluate the membrane's ability to restore its filtration performance after cleaning with 40 °C DI water for half an hour, the initial average water flux of the pristine membrane (J1) was calculated using a DI water feed solution and seawater draw solution under 4 bar applied pressure for a 2-h duration. The average water flux of the groundwater (J_f) was calculated, followed by a thorough rinsing of the membrane with deionized (DI) water at 40 °C for 30 min. After rinsing, the average water flux of the DI water (J_2) was measured. The reversible and irreversible membrane fouling were determined using Eqs. 3 and 4. Total fouling was calculated according to Eq. 5, while the water flux recovery ratio (Frr) was computed using Eq. 6 as the ratio of J_2 to J_1.

$$Rr(\%) = \left(\frac{J2 - Jf}{J1}\right) \times 100 \tag{3}$$

$$Rir(\%) = \left(\frac{J1 - J2}{J1}\right) \times 100 \tag{4}$$

$$Rt(\%) = \left(1 - \frac{Jf}{J1}\right) \times 100 \tag{5}$$

$$Frr(\%) = \left(\frac{J2}{J1}\right) \times 100 \tag{6}$$

2.8. Pore radius and porosity of the membrane

The average theoretical pore radius (R_m) of the membranes was determined by applying the Guerout–Elford–Ferry equation, which quantifies pore size based on membrane permeability characteristics.

$$R_m = \frac{\sqrt{(2{\cdot}90 - 1.75\mathrm{p})8hTF_W}}{\mathrm{p}PA} \tag{7}$$

Where h is the dynamic viscosity of water (Pa·s), F_W is the water flux per unit time, P refers to the applied pressure (MPa), A is the effective membrane area (m^2), T is the thickness of the membrane, and p represents the overall porosity of the membrane and was determined using the equation below:

$$\mathrm{p} = \frac{(\omega_1 - \omega_2)/\rho_\omega}{(\omega_I - \omega_2)/\rho_{w+}\ \omega_2/\rho_\rho} \tag{8}$$

ω_1 and ω_2 represent the weights of the wet and dry membranes, respectively in (g), ρ_ω is the density of water (1.00 g/cm^3), and ρ_ρ represents the density of the membrane polymer.

2.9. Filtration experiments

The PFAS rejection efficiency of the PSRNF membrane was investigated using one litre of PFAS-contaminated groundwater as the feed solution, and one litre of 0.6 M NaCl in DI water at applied pressures of 0, 2, and 4 bar on the feed side. Experiments were conducted until 50 % recovery rates of the feed solution were achieved. Each set of experiments was performed three times, and the average value was reported. Samples of the feed and draw solutions were collected before and after the conclusion of the experiments for PFAS analysis. The PFAS rejection efficiency of the membrane was calculated according to Eq. (2). After the concluding of each experiment, the membrane was removed and stored for further PFAS analysis. Similarly, for fouling assessment, one litre of groundwater was used as the feed solution, and one litre of seawater served as the draw solution. The experiment was operated under an applied pressure of 4 bar for its best water flux performance and was terminated when a 90 % recovery of the feed solution volume was achieved. The procedure was repeated in triplicate, and the average values were reported.

3. Results and discussion

3.1. Role of pressure and pH in PFAS rejection

The PFAS rejection by the PSRNF membrane was assessed under various applied pressures and pH conditions, using a feed solution of one litre of groundwater at pH 4 and a draw solution of one litre of 0.6 M NaCl, resembling seawater concentration. The experiments investigate the influence of operational parameters on the separation of PFAS compounds of different molecular weight classes (long, short, and ultrashort chain species). Experiments were conducted using feed solutions at pH 4, 7, and 9, with applied pressures of 0, 2, and 4 bars on the feed side to stimulate the permeation flux. In each experiment, the

filtration process was terminated upon achieving 50 % recovery of the initial feed volume.

At pH 4 feed solution, a substantial increase in average permeation flux was observed with increasing applied pressure, recording 2.44 L/m^2·h, 16.62 L/m^2·h, and 39.87 L/m^2·h at 0, 2, and 4 bar, respectively (Fig. 2A). The average permeation flux was negligible at 0 bar, primarily due to the lack of applied pressure needed to overcome the membrane's intrinsic hydraulic resistance and initiate water transport. However, the membrane exhibited an exponential responsiveness to slight increases in the applied pressure, owing to its high hydrophilicity and water permeability coefficient [12]. While the average permeation flux showed substantial improvement with a little increase in applied pressure, PFAS rejection varied significantly, where long-chain PFAS such as PFOS, PFDA, PFNA, PFOA, and PFHxS exhibited consistently high rejection, increasing slightly with pressure from 97.2 to 97.9 % at 0 bar, 97.7 to 98.3 % at 2 bar, and 97.8 to 99.2 % at 4 bar (Fig. 2B). Greater rejection of long-chain PFAS compounds is attributed to their larger molecular size and lower solubility, which favour steric hindrance and hydrophobic interactions. PFAS rejection by the PSRNF TS80 membrane is primarily governed by size exclusion and electrostatic repulsion. Size exclusion depends on the molecular weight of the PFAS species compared to the membrane pore size. At the same time, electrostatic interactions result from the repulsion between negatively charged PFAS molecules and the negatively charged polyamide surface of the membrane. Despite the acidic feed environment at pH 4, the long-chain PFAS species remain fully deprotonated due to their very low pK_a values, ensuring their predominantly anionic state at this pH. While the membrane experiences a reduction in surface charge under this acidic condition compared to the neutral condition, it still retains a negative charge that enables electrostatic repulsion to remain an active and relevant rejection mechanism for long-chain PFAS [19]. Another explanation is that elevated pressure can lead to slight membrane compaction, which effectively reduces the membrane pore structure and further enhances PFAS rejection [12].

The membrane exhibited slightly lower rejection efficiencies for the short-chain PFHpA and PFHxA compared to their long-chain counterparts. At 0 bar, PFHpA and PFHxA recorded rejection rates of 93.3 % and 93.1 %, respectively. These values increased slightly as pressure increased to 2 bar, PFHpA rejection rose to 93.9 %, and PFHxA to 93.2 %, while at 4 bar, PFHpA rejection reached 94.1 %, while PFHxA remained unchanged at 93.2 % (Fig. 2B). The ultrashort chain PFAS compounds, particularly TFMS and TFA, exhibited notably distinct rejection behaviours. At 0 bar, the membrane showed compromised rejection of 49.5 % for TFMS and 48.9 % for TFA. However, as the applied pressure increased to 2 bar, TFMS and TFA rejection significantly declined to 44.5 % and 44.1 %, respectively, and then further decreased to 37.9 % for TFMS and 36.7 % for TFA at 4 bar (Fig. 2B). This decline in rejection efficiencies with increasing pressure is likely driven

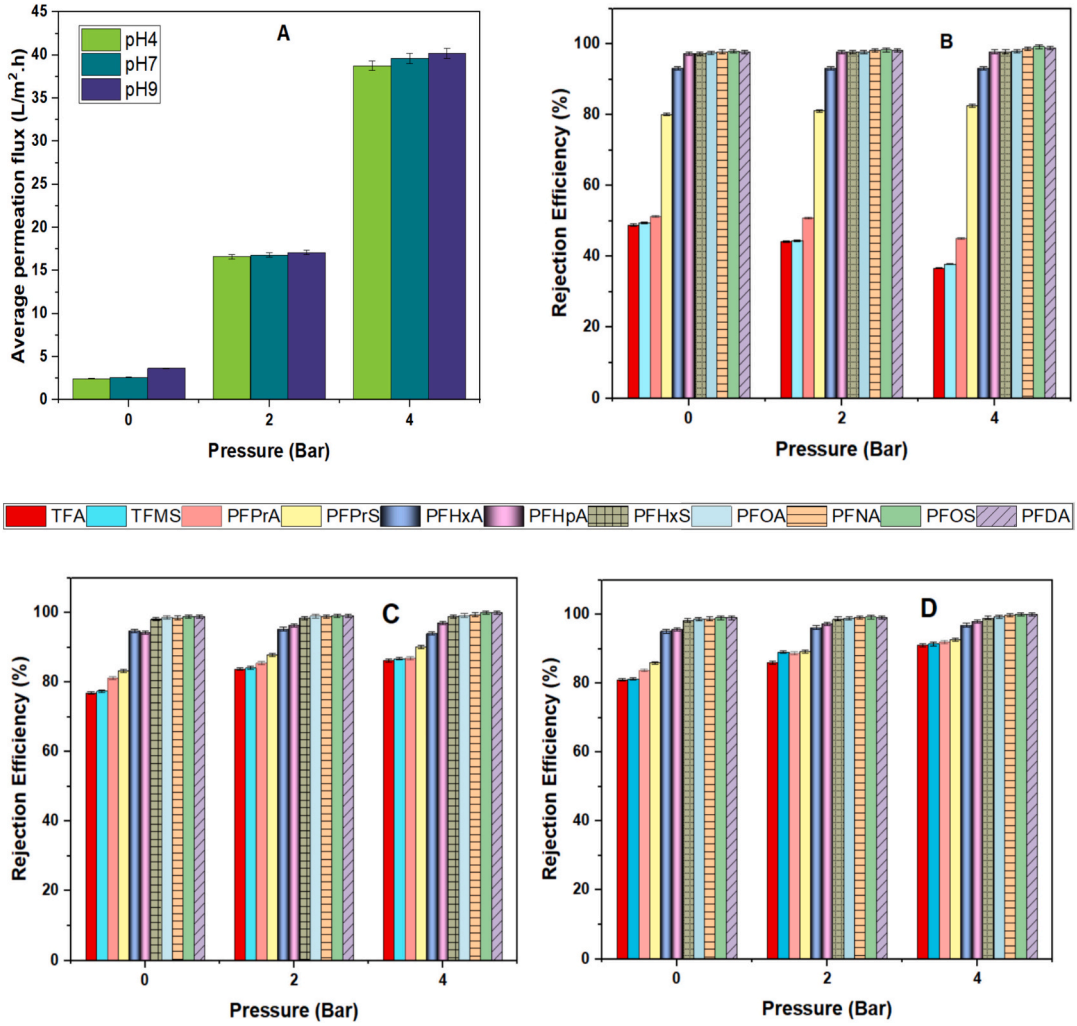

Fig. 2. (A) Average membrane permeation flux at three feed solution pH levels (4, 7, and 9) under applied pressures of 0, 2, and 4 bar; (B) PFAS rejection efficiencies at pH 4 (acidic) under 0, 2, and 4 bar; (C) PFAS rejection efficiencies at pH 7 (neutral) under 0, 2, and 4 bar; (D) PFAS rejection efficiencies at pH 9 (alkaline) under 0, 2, and 4 bar.

by the lower molecular weights, TFMS (~150 g/mol) and TFA (~114 g/mol), which are smaller than long and short-chain PFAS compounds of MW between 114 and 314 g/mol (Table 2). Besides, the small hydrated radii of TFMS and TFA facilitate their passage through the membrane pores under higher pressure. Another reason for the decreased rejection of TFMS and TFA is due to the domination of convective transport compared to diffusive transport as pressure increases, leading to TFMS and TFA molecules getting pushed across the membrane. As pressure increases, these ultrashort-chain PFAS molecules are more readily transported through the membrane due to their limited steric hindrance and minimal charge-based repulsion. Finally, in acidic environments, the membrane surface carries a reduced negative charge, which further weakens repulsive interactions. Consequently, the elevated pressure encourages the diffusion of these small molecules toward the draw solution, reducing the rejection performance [20,21].

To investigate the influence of pH on PFAS rejection, the feed solution was adjusted to pH 7 to resemble neutral alkalinity. Under pH 7, the average permeation flux at all applied pressures (0, 2, and 4 bar) showed a slight increase compared to the previous experiments conducted at acidic pH where average permeation fluxes increased by approximately 2 % at 0 bar (2.61 L/m^2·h), 4 % at 2 bar (16.8 L/m^2·h), and 2.1 % at 4 bar (39.87 L/m^2·h) (Fig. 2A). Long-chain PFAS compounds exhibited a modest increase in rejection with pressure increase, rising from the range of 98.1 to 98.9 % at 0 bar to the range of 98.4 to 99.1 % at 2 bar for PFOS, PFDA, PFNA, PFOA, and PFHxS. At 4 bar feed pressure, the membrane rejection of PFNA, PFOA, and PFHxS further increased to the range from 98.9 to 99.4 %, while there was no trace of PFOS and PFDA, or their concentrations were below the detection limit (Fig. 2C). As the feed solution pH increased to pH 7, the functional groups on the polyamide membrane surface became more ionised, resulting in a stronger negative surface charge. This enhanced surface charge leads to stronger electrostatic interactions between the anionic PFAS species and the membrane's negative surface, thereby improving the rejection rate [22]. Simultaneously, the intensified charge density also increased repulsion between the membrane polymer chains, causing a slight expansion of the membrane matrix. This structural relaxation likely led to a slight increase in effective pore size, which contributed to enhanced water permeability [22]. A comparable improvement was observed in the rejection of short-chain PFAS compounds, PFHpA and PFHxA. Their rejection efficiencies also increased slightly under neutral feed conditions compared to the acidic state, with PFHpA rejection rising from 94.3 % at 0 bar to 96.3 % at 2 bar and 97.1 % at 4 bar. In comparison, the rejection of PFHxA increased from 94.0 % to 94.8 % and 95.3 % at the corresponding pressures. These improvements in rejection are likely driven by the same mechanisms discussed for long-chain PFAS (Fig. 2C). A comparable increase in rejection efficiency was observed for the ultrashort chain PFAS compounds, TFMS and TFA. At pH 7 and 0 bar pressure, TFMS and TFA rejection were 77.4 % and 76.9 %, then rose to 84.1 % and 83.8 % at 2 bar, and further to 86.8 % and 86.2 % at 4 bar (Fig. 2C). The substantial improvement in rejection under neutral conditions compared to the acidic state suggests that electrostatic repulsion plays a dominant role in the separation of ultrashort-chain PFAS by the PSRNF membrane.

Increasing the feed solution pH to 9 shows a slight increase in the average permeation fluxes of approximately 1.5 % at 0 bar (2.65 L/m^2·h), 1.2 % at 2 bar (17.1 L/m^2·h), and 1.4 % at 4 bar (40.21 L/m^2·h) (Fig. 2A) for the same reason discussed above. Similarly, the rejection rate for the long-chain PFAS species showed a slight improvement, ranging from 98.3 to 99 % at 0 bar to 98.7 to 99.2 % at 2 bar for PFOS, PFDA, PFNA, PFOA, and PFHxS (Fig. 2D). At 4 bar, the rejection of PFNA, PFOA, and PFHxS increased, ranging from 99.1 to 99.77 % and no trace concentration was found for the PFOS and PFDA. Short-chain PFAS also showed rejection efficiencies higher compared to the longer chain PFAS, with PFHpA increasing from 95.6 % at 0 bar to 97.2 % at 2 bar and 98 % at 4 bar, while PFHxA increased from 95.08 % to 96.2 % and 96.9 % at the corresponding feed pressures (Fig. 2D). Furthermore, the ultrashort chain PFAS compounds exhibited a notably stronger response to the alkaline environment. Rejection efficiencies for TFMS and TFA increased from 81.3 % and 81.0 % at 0 bar to 89.1 % and 86.0 % at 2 bar and further to 91.4 % and 91.1 % at 4 bar, respectively (Fig. 2D). These results suggest that the enhanced negative surface charge of the membrane under alkaline conditions significantly increases electrostatic repulsion, which improves the rejection of short and ultrashort PFAS species.

Compared to previous studies, the PSRNF membrane used in the FO process achieved a greater rejection rate of a wider range of PFAS compounds in groundwater (Table 3). It showed comparable or slightly higher rejection efficiencies in comparison to NF membranes, including NF90 and NF270, for the rejection of ultrashort-chains (PFPrs), short-chains (PFBA and PFHxA), and long-chains (PFOS and PFHxS). For ultrashort chains PFAS compounds of relatively low molecular weights, i.e., (TFMS and TFA), the PSRNF membrane achieved a 91 % recovery rate at 90 % recovery rate. Long-chain PFAS compounds, such as PFOAS and PFAS, were extensively studies in the literature, with good rejection results by the RO, NF, and FO processes. Ultrashort-chain PFAS compounds, however, were scarcely addressed in the literature, and hence, this study provides insight into their potential treatment by the FO process using the PSRNF membrane.

3.2. Heavy metals removal

Another set of experiments was conducted at pH ranges of 4, 7, and 9 and applied pressures ranging from 0, 2 and 4 bar to investigate the effect of operation conditions on the rejection of heavy metals, such as Al^{3+}, Fe^{2+}, Cu^{2+}, Zn^{2+}, and Mn^{2+}, by the PSR membrane (Table 1). At the acidic condition of pH 4 feed solution, the highest rejection was observed for Al^{3+}, with 91.1 % at 0 bar and increasing to 97.8 % at 4 bar. In contrast, Mn^{2+} exhibited the lowest rejection, ranging from 76.5 % to 83.7 % at the feed pressure ranging from 0 to 4 bar (Fig. 3A). At pH 7, a similar pattern was observed, with Al^{3+} achieving the highest rejection of 92.4 % at 0 bar and 98.9 % at 4 bar, while Mn remained the least rejected, with rejection values improving from 79.5 % to 89.7 % as pressure increased from 0 to 4 bar (Fig. 3B). A combination of steric hindrance and Donnan exclusion governs the rejection of heavy metals by the PSRNF TS80 membrane [27]. Increasing the pH of the feed solution enhances the negative surface charge of the nanofiltration membrane due to the deprotonation of terminal carboxylic groups (–COOH) on the polyamide layer to form $–COO^-$, hence intensifying Donnan exclusion by increasing electrostatic repulsion against positively charged metal ions, thereby improving their rejection [28]. Similarly, increasing the applied pressure leads to higher permeation flux and improved rejection rate due to the greater dilution of the draw solution. In addition, pressure increase leads to a reduction in the pore size and hence enhances steric hindrance. At pH 9, the rejection of Al^{3+} increased from 93.0 % at 0 bar to 99.8 % at 4 bar, reflecting the strong electrostatic repulsion of the highly charged Al^{3+} ions under alkaline conditions. Furthermore, at elevated pH, Al^{3+} may partially hydrolyse to form $Al(OH)_4^-$, which is both larger and more effectively rejected due to size exclusion and electrostatic interaction. In contrast, Mn^{2+} exhibited lower rejection values, but rejection improved from 80.1 % at 0 bar to 90.9 % at 4 bar (Fig. 3C). The relatively lower rejection of Mn^{2+} is attributed to its lower valence and larger hydration shell that is loosely held by the Mn^{2+}. Greater removal of Al^{3+}, Fe^{2+}, Cu^{2+}, and Zn^{2+}compared to Mn^{2+} is attributed to i) smaller charge density of Mn^{2+} compared to Al^{3+}, Fe^{2+}, Cu^{2+}, and Zn^{2+}, ii) larger hydration shell of Al^{3+}, Fe^{2+}, Cu^{2+}, and Zn^{2+} that facilitates their rejection by size exclusion (Table S2). At preference operating condition at pH 9 and 4 bar pressure, the rejection of ions by the PSRNF membrane in the following order: $Al^{3+} \approx Fe^{2+} > Cu^{2+} > Zn^{2+} > Mn^{2+}$.

Table 3
Performance of membranes in PFAS-contaminated wastewater treatment.

Filtration process	Membrane	Module	Feed	PFAS type	Rejection %	Ref
RO	SW30HR–380 (Polyamide TFC)	Flat sheet	Synthetic solution	PFOS & PFOA	>85	[23]
NF	Polyamide	Flat sheet	Synthetic solution	PFHxS	96.9	[24]
				PFHxA	93.4	
NF	NF270–2540 (Polyamide TFC)	Spiral-wound	Groundwater	PFPeA	> 97	[9]
				PFHxA	> 97	
				PFHpA	> 97	
				PFOA	> 97	
				PFPrS PFBS	> 90	
				PFPeS	> 94	
				PFHxS	> 96	
				PFHpS	> 97	
				PFOS	> 97	
					> 98	
NF	NF270	Flat sheet	Synthetic solution	PFBA	94–95	[25]
				PFPeA	97	
				PFHxA	95	
				PFOA	97	
				PFNA	98	
				PFDA	97	
				PFOS	99	
NF	NF90	Flet sheet	Synthetic solution	PFHxA	98	[26]
				PFOA	96	
				PFBS	94	
FO	CTA (FTSH_2O)	Flat sheet	Contaminated soil wastewater	PFOA	99	[22]
FO	TS80	Flat sheet	Groundwater	PFOS	100	This study
				PFDA	100	
				PFNA	99.7	
				PFOA	99.3	
				PFHxS	99.1	
				PFHpA	98	
				PFHxA	96.9	
				PFPrS	92.6	
				PFPrA	92	
				TFMS	91.4	
				TFA	91	

3.3. Membrane surface morphology and chemical properties

A comparative FTIR analysis was performed on the pristine PSRNF membrane and nine post-filtration membrane samples to investigate the impact of operational parameters on membrane surface chemistry (Fig. 4A). Multiple FTIR spectral regions provided essential insights for assessing the chemical interactions and fouling behaviour of the PSRNF membrane across different operational conditions. The pristine membrane spectrum exhibited characteristic bands indicative of polyamide structures, which are essential for confirming the membrane's baseline chemical integrity and composition. The polyamide active layer displayed typical amide bands A at approximately 3300–3500 cm^{-1} corresponding to N—H stretching vibrations, and the distinct Amide *I* and II bands located around 1600–1700 cm^{-1} and 1530–1550 cm^{-1}, respectively, resulting from C═O stretching and N—H bending coupled with C—N stretching vibrations [29]. An observation of some changes were observed in the spectra after filtration, particularly for the membrane operated at 0 bar and pH 4. An intensified and broadened O–H/N–H band suggested increased hydrogen bonding due to the accumulation of hydrophilic foulants such as natural organic matter (NOM) and hydrated metal ions. Enhanced absorbance in the 2950–2850 cm^{-1} region indicated the presence of aliphatic C—H groups, suggesting the deposition of hydrocarbon-rich compounds from NOM. The growth of these peaks confirms the accumulation of organic substances, resulting in fouling layers that alter membrane performance characteristics. It is also important to note that although some PFAS might be present adsorbed in the membrane, no distinctive PFAS-related features were observed in the FTIR spectra due to the weak infrared activity of C—F bonds and the typically low PFAS concentrations, which are easily masked by the dominant signals from the membrane and foulants, making FTIR unsuitable for their direct detection [30]. The observed variations in these spectra are less noticeable for pH 7 and 9 at the same applied 0 bar pressure, which confirms that the membrane is less prone to fouling with increasing pH. These conditions are typically related to a filtration duration and a reduced membrane surface charge at pH 4. At low membrane surface charge conditions, electrostatic repulsion against negatively charged contaminants reduces, enhancing their likelihood of interaction and adsorption onto the membrane surface, which exacerbates fouling.

As the pH increased to 7 and 9, post-filtration membranes showed a decrease in the intensity of the C═O stretching band associated with protonated carboxylic acid groups (–COOH) at around 1700–1725 cm^1. This reduction in intensity indicates the deprotonation of carboxylic acid groups, resulting from the shift in the membrane environment from acidic state to alkaline state. Similarly, an intensified band appeared in the 1400–1450 cm^1 and 1140 cm^1 regions that correspond to the symmetric stretching vibration of carboxylate anions ($–COO^-$), which confirms the conversion of –COOH to $–COO^-$ under alkaline pH, where such a transition contributes to the increased negative surface charge of the polyamide membrane [31]. Compared to the FTIR spectra of the pristine PSRNF membrane, the spectra of the post-filtration membranes did not display the distinctive absorption bands associated with PFAS species, such as the –CFx stretching vibrations near 1327 and 1106 cm^{-1} [32]. This absence indicates that surface adsorption of PFAS on the membrane after filtration was not detected by the FTIR.

SEM images and EDX analyses of the nine post-filtration PSRNF membrane samples revealed variations in fouling on the active layer of the membrane samples, driven by operational conditions. The most observed foulant was at the 0 bar and pH 4, while the least foulant was observed at 4 bar and pH 9 (Figs. S1a-i and S2a-i) as a result of the physicochemical interactions between the membrane surface chemistry, groundwater characteristics and hydrodynamic environment at the membrane surface. As the membrane polyamide layer becomes protonated in acidic conditions, it leads to weakening of the electrostatic

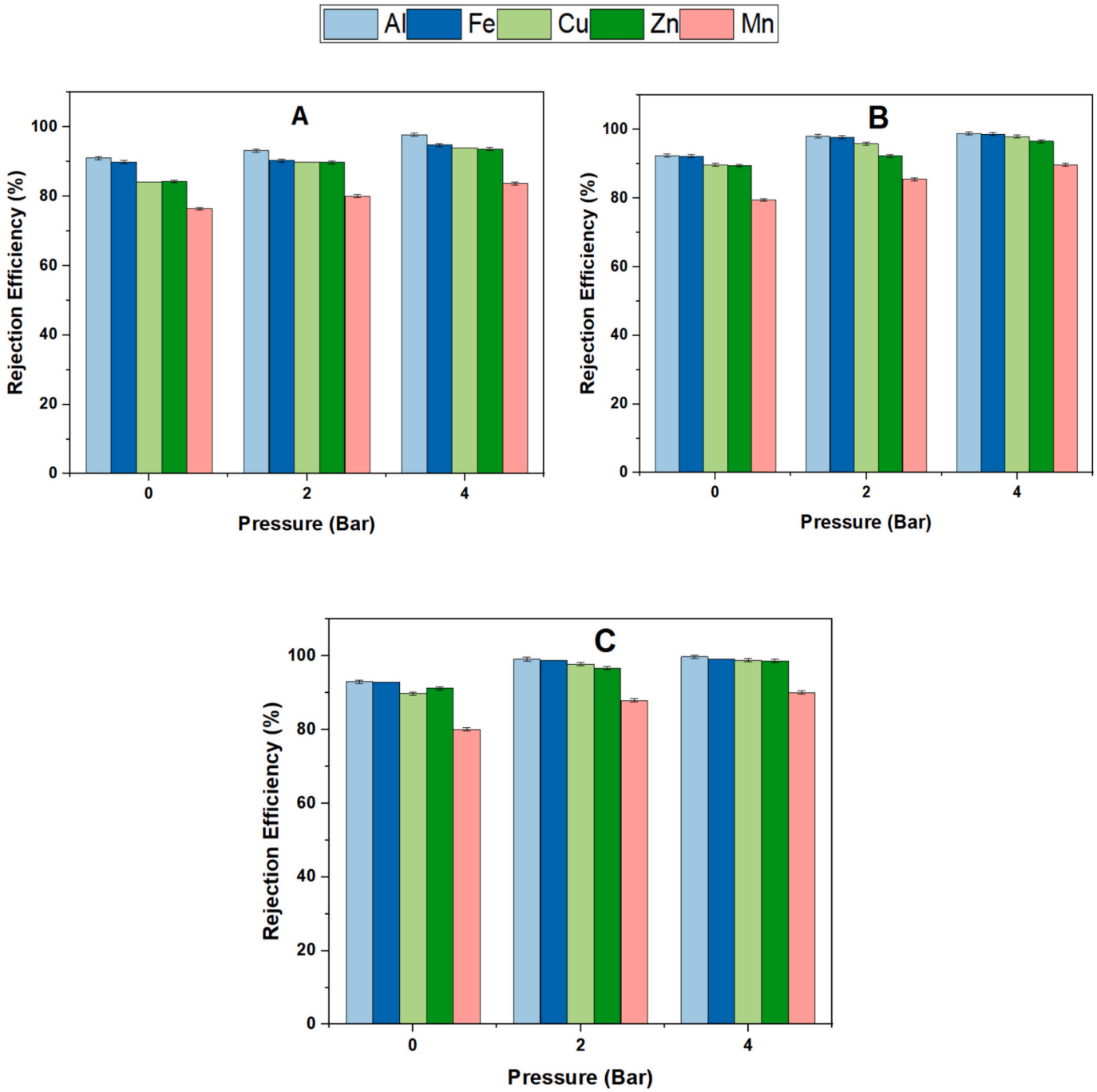

Fig. 3. Heavy metal removal efficiency of the PSRNF membrane under applied pressures of 0, 2, and 4 bar at different feed solution pH levels: (A) pH 4, (B) pH 7, and (C) pH 9.

repulsion between the membrane and various dissolved foulants in groundwater, promoting the adhesion of the latter. The absence of applied pressure reduces shear forces at the membrane active layer. Also, it extends the filtration time (42 h to achieve a 50 % recovery rate), further exacerbating the accumulation of foulants. At an applied pressure of 4 bar and an alkaline state of 9 pH, the least fouling was experienced, resulting from the deprotonation of the membrane functional groups, which leads to a higher negative surface charge that enhances repulsion against charge foulants and improves resistance to adhesion. Additionally, increasing the applied pressure to 4 bar further enhances water flux and shear at the membrane surface, thereby shortening foulant residence time at the membrane surface.

SEM cross-section images of the membrane following filtration at 4 bar (selected due to its higher water flux) with different groundwater pH levels showed that increasing pH levels of the groundwater feed led to a slight increase in the active layer thickness of the membrane. At pH 4, the thickness of the active layer was measured at 143 nm, then increased to 171 nm at pH 7, and further to 192 nm at pH 9 (Fig. 4B, C, and D). This slight expansion in the selective layer likely resulted from the enhanced electrostatic repulsion between ionised functional groups within the membrane matrix, which leads to a slight expansion of the polymer network with increasing pH. These findings also align with the slight increases in water flux observed with increasing pH, which has been discussed in section 3.1.

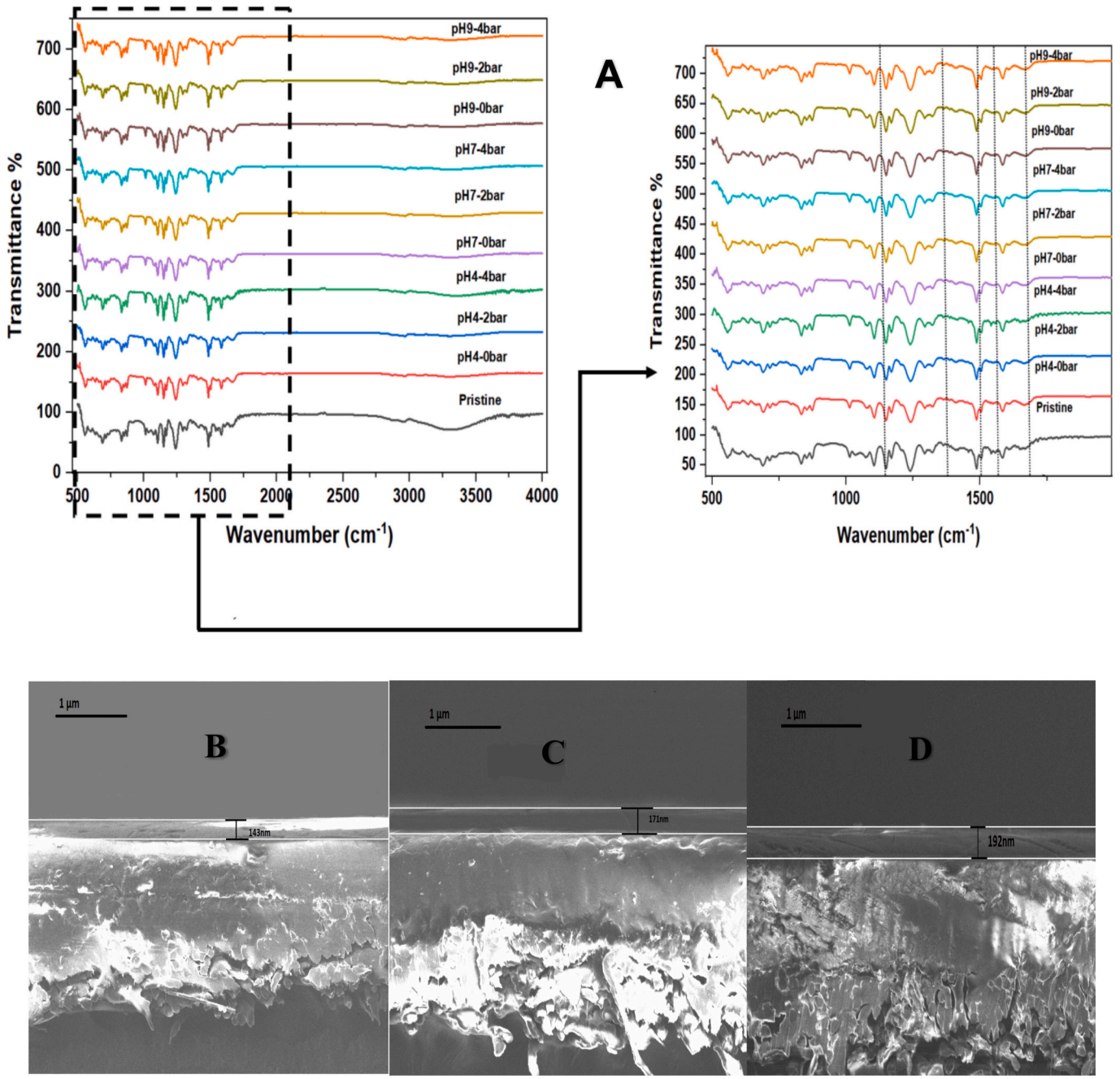

Fig. 4. (A) FTIR spectra of the pristine PSRNF membrane and post-filtration membranes under nine operational conditions varying in pH and applied pressure. (B, C, D) SEM cross-sectional images of the PSRNF membrane showing active layer thickness after filtration at 4 bar and pH levels of 4, 7, and 9, respectively.

3.4. Adsorptive behaviour of PFAS at the membrane surface

To examine the influence of operating conditions, i.e., pressure and feed solution pH, on the membrane adsorption behaviour of PFAS of various chain lengths, membrane samples were collected and analysed. Results showed that adsorption for long-chain PFAS was the highest, followed by short-chain and then ultrashort-chain species under various operational conditions, while increasing pressure and feed solution pH were both associated with a reduction in overall PFAS adsorption. At 0 bar applied pressure, the adsorption of the long-chain was approximately 9.0 %, 8.01 %, and 6.7 % for pH 4, 7, and 9, respectively, while the short-chain showed less adsorption of 5.0 %, 3.9 %, and 3.1 % under the same pH conditions. However, the ultrashort-chain exhibited the lowest adsorption results of 1.4 % and 0.08 % at pH 4 and 7, respectively, and no sign of adsorption at pH 9 or below the detectable limit (Fig. 5A). Increasing applied pressure to 2 and 4 bar further reduced PFAS adsorption across all chain lengths (Fig. 5B and C), recording approximately 9.0 %, 8.01 %, and 6.7 % at pH 4, 7, and 9, respectively, while the short chain showed less adsorption of 5.0 %, 3.9 %, and 3.1 % under the same pH conditions. The ultrashort-chain exhibited the lowest adsorption results of 1.4 % and 0.08 % at pH 4 and 7, respectively, and no sign of adsorption at pH 9 or below the detectable limit (Fig. 5A). Increasing applied pressure to 2 and 4 bar further reduced PFAS adsorption across all chain lengths (Fig. 5B and C). Long-chain PFAS exhibit higher adsorption onto polyamide-based PSR membrane compared to their short and ultra-short chain counterparts. This adsorption behaviour disparity is attributed to the molecular architecture of long-chain PFAS, which is characterised by extended

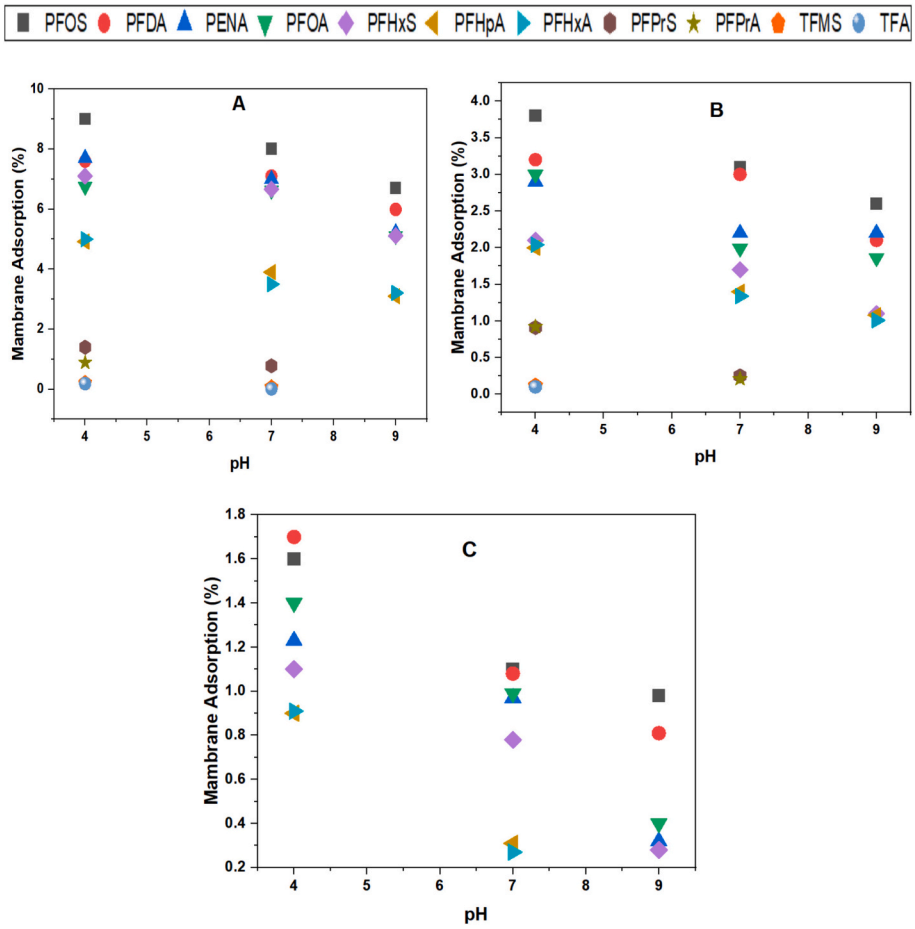

Fig. 5. Adsorption of PFAS species (long, short, and ultrashort-chain) onto the membrane at three feed solution pH levels (4, 7, and 9), under varying applied pressures: (A) 0 bar, (B) 2 bar, and (C) 4 bar. Each graph illustrates adsorption performance across all three pH conditions at the specified pressure.

perfluoroalkyl tails that confer higher hydrophobicity. Increasing hydrophobicity promotes stronger van der Waals forces and fluorophilic interactions with the hydrophobic domains of the polyamide membrane matrix [33].

In contrast, short and ultra-short chain PFAS possess lower hydrophobicity, which limits their affinity for the membrane surface and results in reduced adsorption [34]. As the applied pressure increases, the interaction between the PFAS species and the membrane surface reduces, due to a higher permeation flux and consequently, a shorter residence time within the membrane's boundary layer. This effect disproportionately reduces the adsorption of PFAS, especially for PFAS species with higher hydrophobicity that would otherwise exhibit higher adsorption. Increasing the feed solution pH increases the surface charge of the membrane (more negatively charged), which enhances electrostatic repulsion against anionic PFAS species. These dual effects of increased pressure and alkalinity significantly curtail adsorption, particularly for ultra-short chain PFAS. At 4 bar applied pressure and pH levels of 4,7, 9, there was no detectable adsorption of ultra-short chain compounds recorded. It may be attributed to their inherently low hydrophobicity and short perfluoroalkyl chains, which provide minimal capacity for van der Waals or hydrophobic interactions with the polyamide membrane matrix. At pH 7 and 11, PFAS remains fully deprotonated and thus carries a strong negative charge, leading to pronounced electrostatic repulsion from the negatively charged membrane surface. The combined increase in hydraulic pressure and pH significantly reduces PFAS adsorption across all chain lengths, with the effect being most pronounced for ultra-short chain PFAS. Under alkaline and high-pressure conditions, these species exhibit no detectable adsorption due to their low hydrophobicity, high diffusivity, strong electrostatic repulsion, and limited potential for interactions with the membrane surface. These results highlight the critical influence of PFAS chain length, membrane surface charge, and contact time in determining adsorption behaviour in nanofiltration processes.

3.5. *Membrane fouling and pore size characterisation*

A series of controlled tests was carried out using the PSRNF membrane and contaminated groundwater to assess membrane fouling and potential alterations in membrane pore size during filtering. Pure water flux measurements were conducted before and after each filtering cycle to assess performance variability. A reference test was initially conducted utilising a pristine membrane, with DI water as the feed and seawater employed as the draw solution, under a feed side pressure of 4 bar. This initial test yielded an average water flux of 48.95 L/m^2·h (Fig. 6A) and a corresponding recovery rate of 90 %. The membrane pore size was calculated to be 21.3 nm using Eq. (7). The same membrane was then used to filter groundwater under the same operational conditions until a recovery rate of 90 % was reached, and the average permeate flux was calculated to be 40.2 L/m^2·h (Fig. 6A). The membrane was washed with 40 °C DI water for thirty minutes after the first groundwater filtration cycle to remove any buildup of fouling and loosely attached contaminants [12]. A second test of the DI water feed solution was conducted, resulting in an average permeation flux of 47.55 L/m^2·h (Fig. 6A) and a pore size of 21.28 nm. This sequence of groundwater filtration, followed by membrane cleaning and DI water-seawater FO testing, was repeated in cycles two and three. In the

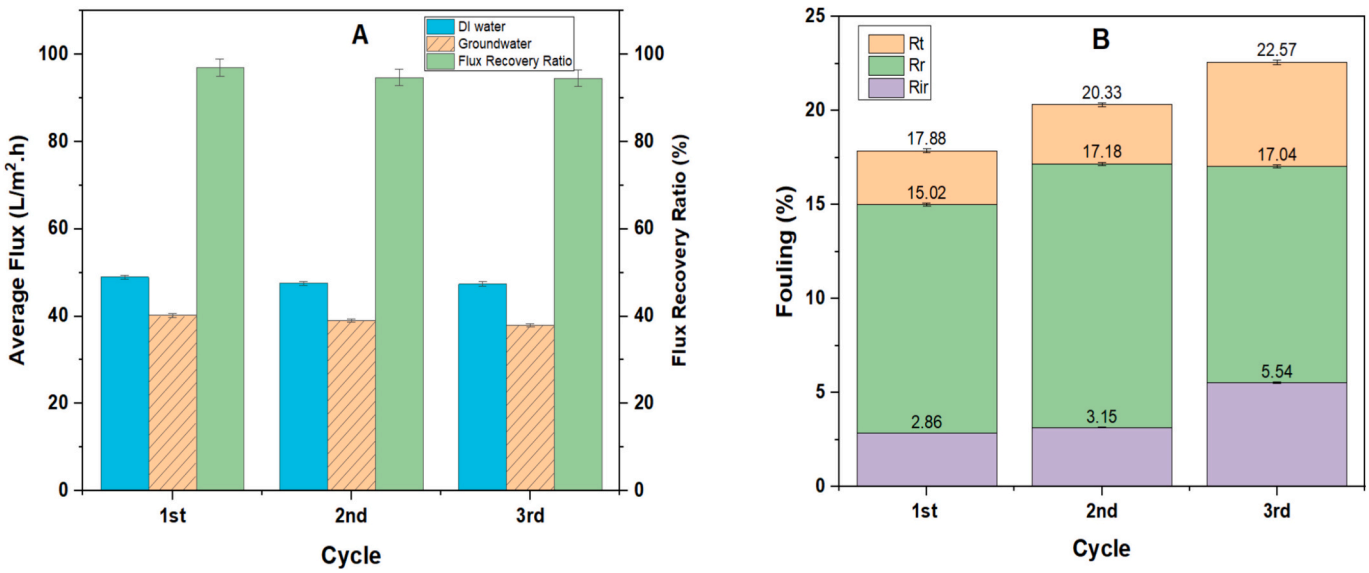

Fig. 6. (A) Average permeation flux for DI water and groundwater, and flux recovery ratio (FRR) measured across three consecutive cycles. (B) Reversible fouling ratio (Rr), irreversible fouling ratio (Rir), and total fouling ratio (Rt) over three consecutive filtration cycles.

second groundwater filtration cycle, the average water flux was 39.00 L/m^2·h, approximately 2.98 % less than that in the first filtration cycle (Fig. 6A). The membrane was rewashed, and a third DI water average water flux test was conducted, yielding an average water flux of 47.41 L/m^2·h and an estimated pore size of 21.26 nm. A third groundwater filtration cycle was then performed, with a reduction of the average water flux to 37.90 L/m^2·h, about 2.82 % less than in the second cycle. Then, after the membrane was cleaned with 40 °C DI water for thirty minutes, a DI water flux test was conducted, resulting in an average flux of 46.24 L/m^2·h and a pore size of 21.24 nm. Throughout the filtration cycles, a slight reduction in pore size was observed during groundwater treatment, associated with the accumulation of irreversible foulants that partially blocked the membrane pores. Washing the membrane with 40 °C DI water was an effective method for restoring up to 97 % and 94.7 % of the membrane's average water flux in the second and third cycles, respectively (Fig. 6A), and the pore size returned close to its original value.

To assess the PSRNF membrane tolerance to fouling and cleaning during groundwater treatment, Rr, Rir, and Rt were assessed after each filtration and cleaning cycle using Eqs. 6–9. In the first filtration cycle, total fouling was calculated at 17.88 %, of which 15.02 % was reversible following the cleaning process, while only 2.86 % was identified as irreversible (Fig. 6B). Total fouling increased to 20.33 % for the second cycle, comprising 17.18 % reversible and 3.15 % irreversible fouling. By the third cycle, total fouling reached 22.57 % including 17.04 % reversible and 5.54 % irreversible fouling, while the flux recovery ratio decreased to 94.46 %. The findings indicate that the majority of the fouling was reversible and could be efficiently mitigated with a straightforward 40 °C DI water wash.

4. Conclusion

This study investigated the PSRNF TS80 membrane performance in removing PFAS species from contaminated groundwater under varying feed pH and applied pressure operational conditions. Due to Steric hindrance and electrostatic repulsion, long- and short-chain PFAS exhibited high removal rates, with rejection efficiencies of 97.9 % and 93.3 % at pH 4 and 0 bar. As the applied pressure increased to 2 and 4 bar, the rejection of long- and short-chain PFAS further improved, reaching 99.2 % and 93.9 %, respectively, due to the increased water flux. In contrast, ultra-short-chain species showed not only low removal efficiency in acidic environments but also further reduction with increasing applied pressure. Nevertheless, their rejection efficiency improved significantly at pH 9, reaching 91.4 % due to enhanced electrostatic repulsion. The findings demonstrated that PFAS rejection is strongly influenced by size exclusion and electrostatic repulsion for both long- and short-chain species. In contrast, ultra-short species are mainly affected by charge repulsion, which occurs at alkaline pH levels. Under acidic and low applied pressure conditions, long-chain PFAS showed a tendency for adsorption on the membrane surface, resulting from a low surface charge that enhances hydrophobic interactions and extends filtration time. The Ultra-short species showed no adsorption across all conditions due to their low hydrophobicity and minimal affinity for the membrane surface. The rejection of heavy metals is also dependent on pH and applied pressure. Al^{3+}, Fe^{2+}, Cu^{2+}, and Zn^{2+} were rejected more effectively under alkaline conditions as they were more likely to form larger hydrolysed species.

The findings of this study highlight the PSRNF membrane's potential for treating PFAS and heavy metals-contaminated groundwater by the forward osmosis process. High rejection efficiency, low energy consumption, and excellent fouling resistance show the potential advantages that contribute to extended operational longevity and reduction in treatment costs. These advantages should be further investigated in a pilot study.

Declaration of competing interest

The authors state no conflict of interest. Ho Kyong Shon serves as a Co-Editor-in-Chief of the journal Desalination, but the editorial handling and peer review of this manuscript were managed by a different Co-Editor-in-Chief.

Acknowledgement

The authors would like to acknowledge the research training program scholarship awarded to Yahia Aedan by the Government of Australia. Viktoria Mueller thanks Faculty of Science Uni Graz and the NAWI Visiting Awards for High Potentials program.

This research is made possible by a food security research award (MME04-0607-230061) from the Qatar National Research Fund (QNRF) in partnership with the Ministry of Municipality.

Appendix A. Supplementary data

Supplementary data to this article can be found online at https://doi.org/10.1016/j.desal.2025.119425.

Data availability

Data will be made available on request.

References

[1] Wang, Z., et al., *A never-ending story of per-and polyfluoroalkyl substances (PFASs)?* 2017, ACS Publications, Environ. Sci. Technol..

[2] H.A. Langberg, et al., Paper product production identified as the main source of per-and polyfluoroalkyl substances (PFAS) in a Norwegian lake: Source and historic emission tracking, Environ. Pollut. 273 (2021) 116259.

[3] F. Cappelli, et al., Occurrence of short-and ultra-short chain PFAS in drinking water from Flanders (Belgium) and implications for human exposure, Environ. Res. 260 (2024) 119753.

[4] R.M. Janousek, J. Mayer, T.P. Knepper, Is the phase-out of long-chain PFASs measurable as fingerprint in a defined area? Comparison of global PFAS concentrations and a monitoring study performed in Hesse, Germany from 2014 to 2018, TrAC Trends Anal. Chem. 120 (2019) 115393.

[5] M.K. Björnsdotter, et al., Ultra-Short-Chain Perfluoroalkyl Acids Including Trifluoromethane Sulfonic Acid in Water Connected to Known and Suspected Point Sources in Sweden, Environ. Sci. Technol. 53 (19) (2019) 11093–11101.

[6] M. Kotthoff, et al., Perfluoroalkyl and polyfluoroalkyl substances in consumer products, Environ. Sci. Pollut. Res. 22 (2015) 14546–14559.

[7] V. Franke, et al., The Price of Really Clean Water: Combining Nanofiltration with Granular Activated Carbon and Anion Exchange Resins for the Removal of Per- And Polyfluoralkyl Substances (PFASs) in Drinking Water Production, ACS ES&T Water 1 (4) (2021) 782–795.

[8] Q. Ma, et al., Evaluation of commercial nanofiltration and reverse osmosis membrane filtration to remove per-and polyfluoroalkyl substances (PFAS): Effects of transmembrane pressures and water matrices, Water Environ. Res. 96 (2) (2024) e10983.

[9] C.J. Liu, T.J. Strathmann, C. Bellona, Rejection of per- and polyfluoroalkyl substances (PFASs) in aqueous film-forming foam by high-pressure membranes, Water Res. 188 (2021) 116546.

[10] Y. Zhi, et al., Enhancing rejection of short-chain per- and polyfluoroalkyl substances by tailoring the surface charge of nanofiltration membranes, Water Res. 272 (2025) 122931.

[11] ChemBK, PFHPA - Physico-chemical Properties, Available from, https://www.chembk.com/en/chem/PFHPA, 2015.

[12] Y. Aedan, A. Altaee, H.K. Shon, Performance of pressure stimuli-responsive nanofiltration and cellulose acetate forward osmosis membranes for PFOA contaminated wastewater treatment, Sep. Purif. Technol. 364 (2025) 132458.

[13] Thermo Fisher Scientific. Trifluoroacetic Acid (TFA) product information. https://www.thermofisher.com/search/browse/category/us/en/80013745#:~:text=Trifluoracetic%20acid%20is%20an%20organofluorine,mass%20spectrometry%2C%20and%20NMR%20spectroscopy. Accessed September 18, 2025.

[14] P.E. Rakita, Triflic acid and its derivatives, Chim. Oggi–Chem. Today (2004) 48–50.

[15] book, C. *1-Propanesulfonic acid, 1,1,2,2,3,3,3-heptafluoro*, Available from, https://www.chemicalbook.com/ChemicalProductProperty_EN_CB94834901.htm, 2023.

[16] Wikipedia, Perfluorohexanoic acid, Available from, https://en.wikipedia.org/wiki/Perfluorohexanoic_acid#, 2025.

[17] D.C. Burns, et al., Experimental p K a determination for perfluorooctanoic acid (PFOA) and the potential impact of p K a concentration dependence on laboratory-measured partitioning phenomena and environmental modeling, Environ. Sci. Technol. 42 (24) (2008) 9283–9288.

[18] R.D. Brook, et al., Air pollution and cardiovascular disease: a statement for healthcare professionals from the Expert Panel on Population and Prevention Science of the American Heart Association, Circulation 109 (21) (2004) 2655–2671.

[19] R.S. Roth, et al., *Effect of solution ions on the charge and performance of nanofiltration membranes.* npj Clean, Water 7 (1) (2024) 25.

[20] M.O. Mavukkandy, et al., Thin film deposition techniques for polymeric membranes– A review, J. Membr. Sci. 610 (2020) 118258.

[21] S. Yi, et al., Application of response surface methodology and central composite rotatable design in optimizing the preparation conditions of vinyltriethoxysilane modified silicalite/polydimethylsiloxane hybrid pervaporation membranes, Sep. Purif. Technol. 71 (2) (2010) 252–262.

[22] Y. Aedan, et al., Perfluorooctanoic acid-contaminated wastewater treatment by forward osmosis: Performance analysis, Sci. Total Environ. 934 (2024) 173368.

[23] H. Hara-Yamamura, et al., Rejection of perfluorooctanoic acid (PFOA) and perfluorooctane sulfonate (PFOS) by severely chlorine damaged RO membranes with different salt rejection ratios, Chem. Eng. J. 446 (2022) 137398.

[24] J. Ma, et al., MXene (Ti3T2CX)-reinforced thin-film polyamide nanofiltration membrane for short-chain perfluorinated compounds removal, Process. Saf. Environ. Prot. 168 (2022) 275–284.

[25] T.D. Appleman, et al., Nanofiltration and granular activated carbon treatment of perfluoroalkyl acids, J. Hazard. Mater. 260 (2013) 740–746.

[26] M. Li, et al., Removal mechanisms of perfluorinated compounds (PFCs) by nanofiltration: Roles of membrane-contaminant interactions, Chem. Eng. J. 406 (2021) 126814.

[27] M. Mullett, R. Fornarelli, D. Ralph, Nanofiltration of mine water: impact of feed pH and membrane charge on resource recovery and water discharge, Membranes 4 (2) (2014) 163–180.

[28] B. Mi, M. Elimelech, Chemical and physical aspects of organic fouling of forward osmosis membranes, J. Membr. Sci. 320 (1) (2008) 292–302.

[29] C.Y. Tang, Y.-N. Kwon, J.O. Leckie, Effect of membrane chemistry and coating layer on physiochemical properties of thin film composite polyamide RO and NF membranes: I. FTIR and XPS characterization of polyamide and coating layer chemistry, Desalination 242 (1) (2009) 149–167.

[30] J. Kumar, M. Narayan, Advanced Nanoformulations for Detection and Removal of Poly-and Perfluoroalkyl Substances (PFAS), Pollutants 5 (2) (2025) 10.

[31] I.M. Kolangare, et al., Improved desalination by polyamide membranes containing hydrophilic glutamine and glycine, Environ. Chem. Lett. 17 (2019) 1053–1059.

[32] N. Stavinski, et al., Unraveling Hidden Infrared Spectral Signatures in PFAS Thermal Degradation with Two-Dimensional Correlation Spectroscopy, Environ. Sci. Technol. Lett. 12 (5) (2025) 668–676.

[33] J. Welchert, et al., Investigation into the adhesion properties of PFAS on model surfaces, RSC Appl. Interfaces 1 (6) (2024) 1265–1275.

[34] S. Das, A. Ronen, A review on removal and destruction of per-and polyfluoroalkyl substances (PFAS) by novel membranes, Membranes 12 (7) (2022) 662.